Acoustic Analogue of Graphene: Observation of Dirac Cones in Acoustic Surface Waves

Daniel Torrent and José Sánchez-Dehesa*

Wave Phenomena Group, Universitat Politècnica de València, Camino de vera s.n. (Edificio 7F), ES-46022 Valencia, Spain

(Received 25 November 2011; published 27 April 2012)

We demonstrate the presence of Dirac cones in the dispersion relation of acoustic waves propagating on the surface of a plate of methyl methacrylate containing a honeycomb lattice of cylindrical boreholes. This structure represents the acoustic analogue of graphene, the cylindrical cavities playing the role of carbon atoms while acoustic surface waves are the equivalent of electronic waves in graphene. Analytical expressions for the Dirac frequency and Dirac velocity in acoustics are given as a function of the radius and depth of boreholes. These parameters have been experimentally determined for a constructed structure and the data are in fairly good agreement with the predicted values.

DOI: 10.1103/PhysRevLett.108.174301 PACS numbers: 43.20.+g, 41.20.Jb

Graphene is a monolayer of carbon atoms densely packed in a honeycomb lattice [1]. Among other interesting properties, the electronic dispersion relation near the corners of the hexagons forming the Brillouin zone (BZ) becomes conical and the dynamics of electrons can be described by Dirac's equation for massless relativistic particles [2]. This feature in the dispersion relation, where two bands touch as a pair of cones, is referred as *Dirac cones* and the touching point as the *Dirac point*. This conical singularity has important symmetry properties and it is the responsible of relevant electronic effects like Andreev reflection and Klein's tunneling [3], *Zitterbewegung* (''trembling motion'') [4] and negative refraction [5].

Dirac cones appear not only in the electronic bands of graphene, but also in the dispersion relation of electromagnetic (EM) waves propagating trough periodic dielectric structures, for example, in two dimensional (2D) photonic crystals [6–9], as well as for three dimensional (3D) photonic crystals [10–13]. Many interesting applications of these EM structures have been reported, like optical waveguides with broken time-reversal symmetry [14], photonic analogues of quantum-Hall effects [15] and positive-zero-negative metamaterials [16].

Dirac cones have been also characterized in the dispersion relation of acoustic waves propagating in a 2D hexagonal lattices of rigid cylinders embedded in water, where the phenomenon of extremal transmission through finite slabs have been analyzed [17]. Recently, a monolayer of silica spheres in water has been proposed as an acoustic analog of graphene and its dispersion relation has been theoretically studied [18]. However, no experimental determination of the dispersion relation near the Dirac point has been reported up to date and the dynamics of acoustic waves near the Dirac point has not been analyzed till now.

In this Letter we demonstrate analytically and confirm experimentally the presence of Dirac cones in the dispersion relation of acoustic waves propagating on a surface containing a honeycomb lattice of cylindrical boreholes drilled in a plate of methyl methacrylate (Plexiglas). We will show that the structure of perforated cavities and the surface acoustic waves that they subtend represent the acoustic analogues of carbon atoms and electronic waves, respectively, in graphene. Analytical expressions of the parameters defining the cone—the Dirac frequency and the Dirac velocity—have been obtained as a function of the cavity parameters (radius and depth). Moreover, we also demonstrate that the secular equation near the Dirac point is equivalent to the 2D Dirac equation for massless relativistic particles, but being the radius and depth of the boreholes the parameters that are analogous to the electrostatic potential. Our model predictions are supported by a direct measurement of the dispersion relation of the acoustic surface waves.

Figure 1 shows the scheme of the honeycomb lattice of boreholes drilled in a Plexiglas plate, which behaves as an acoustically rigid solid (no elastic waves are excited inside it). This crystalline structure is obtained by repeating the hexagonal unit cell containing two identical boreholes α and β. The primitive vectors $\boldsymbol{a}_1$ and $\boldsymbol{a}_2$ define the unit cell and the presence of two equivalent scatterers creates, as it is shown later, a doubly degenerated band structure, responsible of the presence of Dirac cones at the edges of the Brillouin zone as in the case of electronic graphene.

Let us start with the acoustic analogue of electrons traveling in graphene. They are acoustic waves confined in the plate's surface. Therefore, for a frequency ω, we seek for wave solutions confined in the surface, $z = 0$, with the form

$$\psi(\mathbf{r}_{||}, z; \omega) = \sum_{\boldsymbol{G}_{||}} A_{\boldsymbol{G}} e^{-\Gamma_G z} e^{i(\boldsymbol{G}_{||}+\boldsymbol{K}_{||})\cdot \boldsymbol{r}_{||}}, \qquad z \geq 0, \quad (1)$$

where $\boldsymbol{G}_{||} = h_1\boldsymbol{b}_1 + h_2\boldsymbol{b}_2$ represent the vector of the reciprocal lattice, $\boldsymbol{b}_1$ and $\boldsymbol{b}_2$ are the primitive vectors in the reciprocal space, and $\boldsymbol{K}_{||} = \boldsymbol{K}_{||}(\omega)$ represents 2D Bloch's wave vectors.

The guiding characteristics of the acoustic surface waves is preserved when

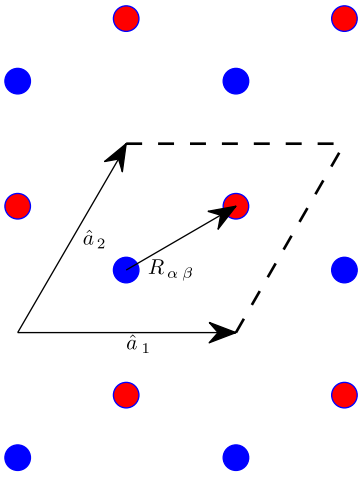

FIG. 1 (color online). Schematic view of the acoustic graphene studied in this work. It consists of a honeycomb lattice of boreholes drilled in a rigid plate. a_1 and a_2 represent the primitive vectors of the hexagonal unit cell containing two acoustic cavities. The distance between nearest neighbors $d = |\boldsymbol{R}_{\alpha\beta}| = a/\sqrt{3}$, where $a = |\mathbf{a}_1| = |\mathbf{a}_2|$.

$$\Gamma_{\boldsymbol{G}}^2 = |\boldsymbol{G}_{||} + \boldsymbol{K}_{||}|^2 - (\omega/c_b)^2 > 0, \tag{2}$$

being c_b the speed of sound in air. This condition limits the solutions to values inside the so-called "light cone" $|\boldsymbol{K}_{||}(\omega)| > \omega/c_b$.

For the pressure field inside the boreholes cavities we consider that only the fundamental mode is excited [19] and therefore

$$\psi_{\alpha(\beta)}(z;\omega) = B_{\alpha(\beta)} \cos\frac{\omega(L+z)}{c_b}, \tag{3}$$

where the subindex α and β represent the two types of boreholes inside the unit cell and L is their depths. Since the plate is rigid we consider that $\partial_z \psi_i(z = -L) = 0$, for $i = \alpha, \beta$.

In order to obtain the band structure we apply the mode matching technique [20] to the unit cell, so that we solve for the $A_{\boldsymbol{G}}$ coefficients and arrive to the following secular equation for the eigenvectors B_α and B_β,

$$\begin{pmatrix} \cot\omega L/c_b - f\chi_{\alpha\alpha} & -f\chi_{\alpha\beta} \\ -f\chi_{\alpha\beta}^* & \cot\omega L/c_b - f\chi_{\alpha\alpha} \end{pmatrix} \begin{pmatrix} B_\alpha \\ B_\beta \end{pmatrix} = 0, \tag{4}$$

where f is the fraction of volume occupied by the cylindrical cavities; that is, the area of the boreholes divided by the area of the unit cell, and $\chi_{\alpha\beta} = \chi_{\alpha\beta}(\omega, \boldsymbol{K})$ are the following overlapping functions,

$$\chi_{\alpha\beta} = \sum_{\boldsymbol{G}_{||}} \frac{k_0}{\Gamma_{\boldsymbol{G}_{||}}} H_\alpha(\boldsymbol{G}_{||}) H_\beta^*(\boldsymbol{G}_{||}) \tag{5}$$

with

$$H_\alpha(\boldsymbol{G}_{||}) = e^{i(\boldsymbol{K}_{||}+\boldsymbol{G}_{||})\cdot\boldsymbol{R}_\alpha} \frac{2J_1(|\boldsymbol{K}_{||} + \boldsymbol{G}|R_0)}{|\boldsymbol{K}_{||} + \boldsymbol{G}_{||}|R_0}, \tag{6}$$

where J_1 are the Bessel function of first order and $k_0 = \omega/c_b$ is the wave number in air (see details in [19]).

The solution of the secular equation (4) is given by the following transcendental equations:

$$\cot\frac{\omega L}{c_b} = (\chi_{\alpha\alpha} \pm |\chi_{\alpha\beta}|) f, \tag{7}$$

where the $\pm$ signs appear as a consequence of having two cavities per unit cell.

These two equations can be solved for a particular pair of values (R_0, L) to generate the corresponding acoustic bands $\omega(\boldsymbol{K}_{||})$ like those shown in Fig. 2 that has been obtained using $R_0 = 0.26a$ and $L = 0.5a$, where a is the lattice constant (see Fig. 1). Only the dispersion relation of guided modes, $|\boldsymbol{K}_{||}| > \omega/c_b$, is shown. The inset shows a zoom at the neighborhood of the Dirac point K, the touching point between the two conical bands. It is in the frequency region near the Dirac frequency, ω_D, where the analogy between surface acoustic waves and electrons in graphene occurs and, therefore, it is the frequency region that will be analyzed in what follows.

The inset in Fig. 2 shows that the dispersion relation becomes linear in the neighborhood of the Dirac point. The linear behavior is clearly observed in the upper branch while, for the lower branch, it becomes linear only near the K point. Therefore, an expansion of the band structure around this point will lead to a linear relation between ω and $\boldsymbol{K}$. The demonstration is too long to be included here, but it is described in the Supplemental Material [19]. In

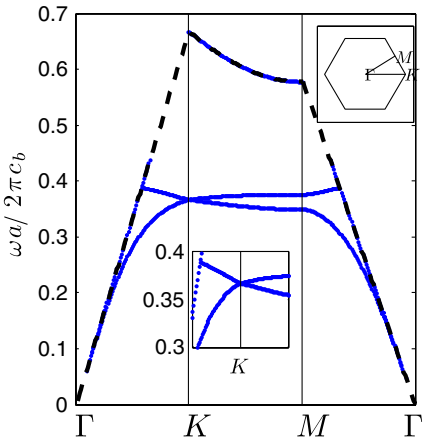

FIG. 2 (color online). Band structure of the acoustic surface waves propagating on a honeycomb lattice of boreholes drilled in a Plexiglas plate. The radius and depth of the boreholes are $R_0 = 0.26a$ and $L = 0.5a$, respectively, where a is the lattice constant of the underlaying hexagonal lattice (see Fig. 1). The upper right inset shows the Brillouin zone with the high symmetry points. The central inset shows a zoom of the dispersion relation around the Dirac point.

brief, the derivation starts with the secular equation (4), where the term $\cot\omega L/c_b$ is expanded up to the first order in $\delta\omega$, where $\delta\omega = \omega - \omega_D$. In the same manner, the terms $\chi_{\alpha\beta}$ are also expanded up to the first order in $\delta\omega$ and $\delta\boldsymbol{K}$, where $\delta\boldsymbol{K} = \boldsymbol{K}_{||} - \boldsymbol{K}_D$. After a lengthy derivation Eq. (4) becomes

$$\begin{pmatrix} \delta\omega/c_D & \delta\boldsymbol{K}\cdot(\hat{\boldsymbol{x}} + i\hat{\boldsymbol{y}}) \\ \delta\boldsymbol{K}\cdot(\hat{\boldsymbol{x}} - i\hat{\boldsymbol{y}}) & \delta\omega/c_D \end{pmatrix}\begin{pmatrix} B_\alpha \\ B_\beta \end{pmatrix} = 0. \quad (8)$$

This equation is the Dirac equation in the 2D momentum space, and it shows that the linear combination of surface waves described by equation (1) can be described, in the neighborhood of the Dirac point $\boldsymbol{K}_D$, by a single wave propagating with wave vector $\delta\boldsymbol{K}$ and satisfying the above equation. Note that to obtain the equation in differential form we should replace $\delta\boldsymbol{K}$ by the differential operator $-i\boldsymbol{\nabla}$, and we will recover the eigenvalue equation with eigenvalues $\delta\omega/c_D$ and eigenvectors B_α, B_β.

The values for the Dirac frequency ω_D and Dirac velocity c_D are obtained from the Taylor expansion of the terms $\chi_{\alpha\beta}$ and some tedious algebra, as explained in [19], where expressions for ω_D and c_D as a function of R_0 and L are obtained.

Figure 3 shows ω_D (upper panel) and c_D (lower panel) as a function of boreholes' depth L/a for a fixed radius $R_0 = 0.26a$. Note that increasing the length L of boreholes decreases either ω_D as well as c_D. The former decreases because the deeper the boreholes, the larger the wavelength of the fundamental mode of the hole, which is related to Dirac frequency through Eq. (7). The later decreases as a direct consequence of the decreasing of Dirac frequency, since this velocity is the slope of the line going from (0, 0) to (K_D, ω_D) in the band structure.

To demonstrate the linear dispersion relation $|\delta\boldsymbol{K}| = \pm|\omega - \omega_D|/c_D$ resulting from Eq. (8), and to confirm the values of ω_D and c_D resulting from our semianalytical theory [19], we have carry out experiments on a Plexiglas plate with cylindrical perforations distributed in a honeycomb lattice. A total of 1113 boreholes were drilled in a plate of dimension 300 × 100 mm. The lattice constant is $a = 5.77$ mm, being the distance between boreholes $d = 3.33$ mm. The radius and depth of the boreholes are $R_0 = 1.5$ mm $= 0.26a$ and $L = 2.88$ mm $= 0.5a$, respectively. With these parameters and using $c_b = 346$ m/s the predicted values of Dirac's frequency and velocity are $\nu_D = \omega_D/2\pi = 22$ kHz and $c_D = 29.06$ m/s. In reduced units, these values correspond to the symbols in Fig. 3, which are $\omega_D a/2\pi c_b = 0.367$ and $c_D = 0.084c_b \approx c_b/12$, which means these waves travels about 12 times slower than they do in free space.

The experimental set up is shown in Fig. 4. The tweeter at grazing incidence excites acoustic surface waves as explained in [21], whose relative phase is measured by two microphones located at 1 mm over the surface. The excited sound field is a Gaussian pulse with central frequency $\nu_0 = 22$ kHz, and width $\Delta\nu = 5$ kHz, so that the predicted Dirac frequency is included in the frequency range of the time signal. A total of 500 averaged spectra are taken by microphones 1 and 2, then from the angle of the cross spectrum the phase delay is obtained.

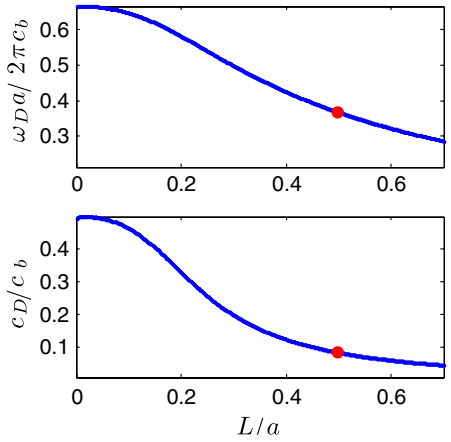

FIG. 3 (color online). Dirac frequency (upper panel) and Dirac velocity (lower panel) as a function of boreholes depth L. Both graphs are obtained for a fixed boreholes radius of $R_0 = 0.26a$. The circles indicates the values at $L = 0.5a$, which is the value used in the sample characterized.

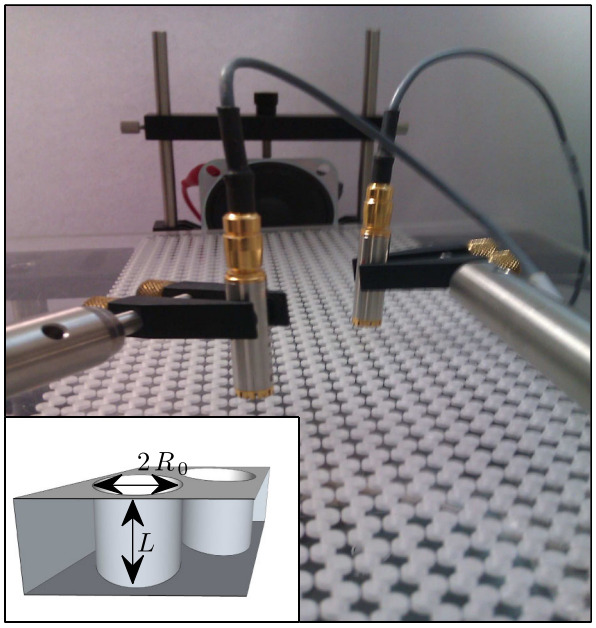

FIG. 4 (color online). Picture of the experimental setup. A loudspeaker at grazing incidence is employed to excite acoustic surface waves propagating on a Plexiglas plate with cylindrical boreholes distributed in a honeycomb lattice. Boreholes appear in the picture as white points due to refraction of light. The inset shows a schematic view of the boreholes geometry. Two microphones located at different points on the surface measure the phase delay between the propagating surface waves.

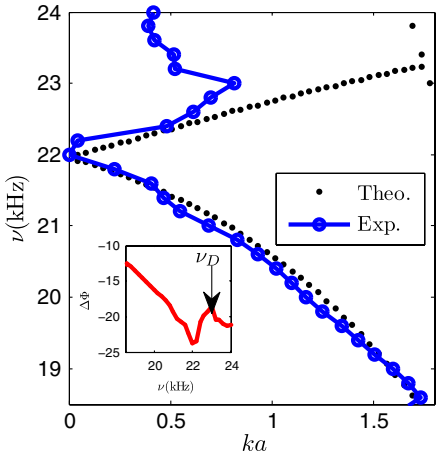

FIG. 5 (color online). Dispersion relation of the acoustic surface waves guided in a Plexiglas plate with a honeycomb array of cylindrical perforations. The inset shows the phase delay between the two microphones employed in the experimental setup (see Fig. 4). Note that the origin of the horizontal axis actually corresponds to the K point of the Brillouin zone.

The inset in Fig. 5 shows the unwrapped phase delay, where it can be observed a minimum near 22 kHz that corresponds to the vertex of the Dirac cone, defining therefore the Dirac frequency. Note the excellent agreement between theory and experiment at the frequencies near the Dirac frequency, where the dispersion relation is clearly linear,

$$k = |\boldsymbol{k}| = 2\pi \frac{|\nu - \nu_D|}{c_D}, \tag{9}$$

where k is the wave number and ν_D is the Dirac linear frequency. The absolute value in the difference between the frequency and the Dirac frequency is the responsible of the local minimum, which is a peculiarity of a Dirac cone. This dispersion can be obtained from the phase delay between the two microphones $\Delta\phi = \Delta\phi(\omega)$ given by

$$\Delta\phi(\omega) = \boldsymbol{k} \cdot \boldsymbol{r}_{12} = |\boldsymbol{k}||\boldsymbol{r}_{12}| \cos(\theta_0 - \theta_{12}), \tag{10}$$

where θ_0 and θ_{12} are the angles between the x axis and vectors $\boldsymbol{k}$ and $\boldsymbol{r}_{12}$, respectively, the last one being the vector going from one microphone to the other one. Note that the phase delay at the Dirac frequency is not necessary an integer of 2π, since the full wave is modulated by a factor $\exp(i\boldsymbol{K}_D \cdot \boldsymbol{r}_{12})$. The symmetry of our setup suggests that three of these angles are possible, $\theta_0 = \pm\pi/3$ and $\theta_0 = 0$, corresponding to the three directions ΓK that can be excited.

Figure 5 shows the dispersion relation obtained in this way as a function of frequency assuming that $\theta_0 = \pm\pi/3$. The fairly good agreement between theory and experiment indicates that this is the dominant mode. Note that frequencies above 23 kHz are outside the "light cone" and, therefore, the measured dispersion relation does not correspond to guided waves. Results below 18 KHz are not displayed because our excitation signal is a Gaussian pulse and that region corresponds to weak time signal with noise playing a dominant role.

In summary, it has been shown that acoustic waves propagating on the surface of an acoustically rigid surface with cylindrical cavities arranged in a honeycomb lattice present a dispersion relation that is similar to that of electrons in graphene. In other words, it is possible to characterize Dirac cones at the edges of the Brillouin zone. Also, we have demonstrated that the dispersion relation near these points can be obtained from a Dirac-like equation and that the Dirac frequency and velocity are functions of the cavity radius and depth. Experimental validation of the theory has been performed by a simple measurement of the phase delay between two points on the surface of a sample constructed with Plexiglas. Since the theory presented here is fully scalable, this work paves the road to translate the interesting phenomena discovered with electrons in graphene to the case of surface acoustic waves propagating in acoustic graphene, which can be fabricated in different length domains, from microscopic to macroscopic dimensions.

Work supported by the Spanish Ministry of Science and Innovation (MICINN) under Contracts No. TEC2010-19751 and No. CSD2008-66 (CONSOLIDER program). Daniel Torrent acknowledges support from the program "Campus de Excelencia Internacional 2010 UPV." Both authors thank Didier Mayou for useful discussions.

*jsdehesa@upvnet.upv.es

[1] K. S. Novoselov, A. K. Geim, S. V. Morozov, D. Jiang, M. I. Katsnelson, I. V. Grigorieva, S. V. Dubonos, and A. A. Firsov, Nature (London) **438**, 197 (2005).
[2] A. H. Castro Neto, F. Guinea, N. M. R. Peres, K. S. Novoselov, and A. K. Geim, Rev. Mod. Phys. **81**, 109 (2009).
[3] C. Beenakker, Rev. Mod. Phys. **80**, 1337 (2008).
[4] M. Katsnelson, Eur. Phys. J. B **51**, 157 (2006).
[5] V. Cheianov, V. Fal'ko, and B. Altshuler, Science **315**, 1252 (2007).
[6] R. A. Sepkhanov, Y. B. Bazaliy, and C. W. J. Beenakker, Phys. Rev. A **75**, 063813 (2007).
[7] X. Zhang, Phys. Rev. Lett. **100**, 113903 (2008).
[8] Z. Wang, Y. Chong, J. Joannopoulos, and M. Soljačić, Phys. Rev. Lett. **100**, 13 905 (2008).
[9] T. Ochiai and M. Onoda, Phys. Rev. B **80**, 155103 (2009).
[10] K. Ishizaki and S. Noda, Nature (London) **460**, 367 (2009).
[11] D. Han, Y. Lai, J. Zi, Z.-Q. Zhang, and C. T. Chan, Phys. Rev. Lett. **102**, 123904 (2009).
[12] W. Zhong and X. Zhang, Opt. Express **19**, 13 738 (2011).
[13] X. Huang, Y. Lai, Z. H. Hang, H. Zheng, and C. T. Chan, Nature Mater. **10**, 582 (2011).

[14] F. Haldane and S. Raghu, Phys. Rev. Lett. **100**, 13 904 (2008).
[15] S. Raghu and F. D. M. Haldane, Phys. Rev. A **78**, 033834 (2008).
[16] M. Shen, L. Ruan, and X. Chen, Opt. Express **18**, 12 779 (2010).
[17] X. Zhang and Z. Liu, Phys. Rev. Lett. **101**, 264303 (2008).
[18] W. Zhong and X. Zhang, Phys. Lett. A **375**, 3533 (2011).
[19] See Supplemental Material at http://link.aps.org/supplemental/10.1103/PhysRevLett.108.174301 for a detailed derivation of the main equations involved in the text.
[20] R. Collin, *Field Theory of Guided Waves* (Wiley, New York, 1991).
[21] L. Kelders, W. Lauriks, and J. Allard, J. Acoust. Soc. Am. **104**, 882 (1998).